INSTITUTE OF PLASMA PHYSICS

NAGOYA UNIVERSITY

RESEARCH REPORT

NAGOYA, JAPAN

Propagation of Nonlinear Ion Acoustic Wave with Generation of Long-Wavelength Waves

Yukiharu Ohsawa and Tetsuo Kamimura

IPPJ-297 July 1977

Further communication about this report is to be sent to the Research Information Center, Institute of Plasma Physics, Nagoya University, Nagoya 464, Japan.

Abstract

The nonlinear propagation of the wave packet of an ion acoustic wave with wavenumber $k_0 \simeq k_{De}$, the electron Debye wavenumber, is investigated by computer simulations. From the wave packet of the ion acoustic wave, waves with long wavelengths are observed to be produced within a few periods for the amplitude oscillation of the original wave packet. These waves are generated in the region where the original wave packet exists. Their Characteristic wavelength is of the order of the length of the wave packet, and their propagation velocity is almost equal to the ion acoustic speed. The long-wavelength waves thus produced strongly affect the nonlinear evolution of the original wave packet.

§1. Introduction

In the fluid model, small-amplitude ion acoustic waves of rather short wavelength are described by a nonlinear Schrödinger equation[1] and so can be shown to be stable against modulational instabilities. However, Ichikawa and Taniuti[2] have constructed a kinetic theory of the nonlinear modulation of the ion acoustic wave which includes the contribution of resonant particles with velocities near the group velocity of the wave while neglecting the effect of resonant particles with velocities near the phase velocity of the wave. They derived a modified nonlinear Schrödinger equation and thus concluded that the ion acoustic wave can indeed become unstable with respect to the modulational instability. Previous experimental and computational studies[3),4)] have shown the importance of trapped particles but did not observe modulational instability.

In the present paper, we report computational results which show that a rather short-wavelength ion acoustic wave produces ion acoustic waves with long wavelengths over a short time scale and that these long-wavelength waves strongly affect the nonlinear behavior of the original wave packet. These results were obtained from an investigation of initial value problem of the wave packet of an ion acoustic wave, where the wavenumber, k_0, of the carrier wave was taken to be $k_0 \simeq k_{De}$, with k_{De} the electron Debye wavenumber. Our results may be summarized as follows. As the wave packet propagates, long-wavelength waves are generated in the region where the original wave packet exists, with characteristic wavelength of the order

of the length of the wave packet. These waves grow during the first few periods of oscillation of the amplitude of the original wave packet, after which the peak value of the long-wavelength waves saturates. Their growth rate in the initial stage is roughly proportional to the square root of the amplitude of the original wave. This suggests that the resonance particles whose velocities are near the phase velocity of the original wave play an important role in the generation of the the long-wavelength waves. Their propagation velocity is almost equal to the sound velocity, c_s, and is faster than both the phase velocity and the group velocity of the original wave which has $k_0 \simeq k_{De}$. Thus, although the long-wavelength waves and the original wave packet initially occupy the same region, the long-wavelength waves gradually move ahead of the wave packet. Also, these waves strongly influence the nonlinear behavior of the original wave packet. Finally, when the original wave is monochromatic and, hence, unmodulated, this generation of long-wavelength waves was not observed.

In §2, the one-dimensional, electrostatic model for the computer simulation[4)] is described. The electrons are assumed to be in a Boltzmann distribution with constant temperature, which eliminates the high-frequency oscillations. Therefore, we can use an integration time step comparable to the characteristic time scale of the ion acoustic wave. For the ions, a hybrid solution algorithm is used[5)] which includes the effects of resonance between the ion particles and the waves. The results of the simulations are presented in §3. Generation of the

long-wavelength waves from the wave packet is shown and studied in detail. In §4, our conclusions are summarized and discussed.

§2. Simulation Model

As was previously mentioned, we consider a one-dimensional, electrostatic problem. The electrons are assumed to have a Boltzmann distribution with constant temperature T_e. For the ions, a hybrid solution algorithm[4),5)] in used, which was originated by Denavit. In this model, the two-dimensional (x, v) phase space is covered with a rectangular grid with mesh size Δx and Δv, initially, weighted simulation particles (ions) are located on the grid points (x_i, v_j) wiht mass and charge proportional to the initial value of the distribution function $f(x_i, v_j)$. The CIC (Cloud in Cell) model[6)] is used for the simulation particles. Then, the simulation particles are advanced along the characteristics of the Vlasov equation, and at a later time the distribution function, f(x, v), is calculated from the locations and masses of the weighted simulation particles.

In our model, the velocity distribution of the particles is replaced by a set of discrete beams. Such a system is known to be subject to the beaming instability[7)], even if the envelope of the beam density is Maxwellian. In a system consisting of an electron fluid and multi-ion beams with a Maxwellian envelope, the growth rate of the beaming instability is given, in the limit of $\Delta v \to 0$, by

$$\gamma_B \simeq (k\Delta v/2\pi)\,|\ln(\Delta v/v_T)| \quad ,$$

where v_T is the ion thermal velocity, $v_T = (T_i/M)^{1/2}$, and k is the wavenumber of perturbations. In order to suppress the beaming instability, we reconstruct the distribution function every N time steps during the course of the simulation run. The time intervals between reconstructions are taken to be short compared to the inverse of the maximum growth rate of the beaming instability, i.e., $N < (\gamma_B \Delta t)^{-1}$, where Δt is the time mesh size. In our simulations, we usually take N to be about 10.

The characteristic mesh sizes, Δv, Δt, and Δx, are chosen to be $\Delta v/v_T \approx 0.06$, $\omega_{pi}\Delta t = 0.2$ and $L/\Delta x \approx 512$, with L being the total system length. Periodic boundary conditions with period L are used. We neglect the particles with velocity $v < -5v_T$ or $7v_T < v$.

Our computations then simulate the two-component plasma described by the following set of equations:

$$\frac{\partial f}{\partial t} + v \frac{\partial f}{\partial x} + \frac{eE}{M} \frac{\partial f}{\partial v} = 0 \quad , \tag{1}$$

$$n_e = n_0 \exp(e\phi/T_e) \quad , \tag{2}$$

$$\partial E/\partial x = 4\pi e(n_i - n_e) \quad , \tag{3}$$

$$E = -\partial\phi/\partial x \quad , \tag{4}$$

$$n_i = \int f(x, v)dv \quad . \tag{5}$$

Here, n_0, n_e, n_i and ϕ are the average plasma density, the electron and ion densities, and the electric potential, respectively. Equation (1) is the Vlasov equation for the ion distribution function. Combining eqs.(2),(3), and (4), we

obtain the equation for the electric field

$$E = -\frac{T_e}{e}\frac{\partial}{\partial x}\{\ln(n_i - \frac{1}{4\pi e}\frac{\partial E}{\partial x})\} \quad . \tag{6}$$

The electric field is numerically solved for by using an implicit iteration scheme[8),9)]. The total conserved energy for our model is given by

$$E_{tot} = \frac{M}{2}\int_L dx \int dv\ fv^2 + \frac{1}{8\pi}\int_L dx\ E^2 + \int_L dx\ n_e e\phi + \text{constant} \ . \tag{7}$$

The scheme described in this section has been previously used to study the frequency shift and nonlinear modulation of ion acoustic waves[3),4)].

§3. Generation of Long-Wavelength Perturbations from Wave Packet

Resonant three-wave interactions[10)] are prohibited for ion-acoustic waves. Hence, nonlinear Landau damping[2),11),12)] has been considered the most important process for energy transfer from a high-frequency ion-acoustic wave to one of lower frequency. Nonlinear Landau damping is described by a third-order perturbation theory, and the characteristic growth rate of the low-frequency wave is proportional to the amplitude of the high-frequency wave[2)], or its square[11),12)], when the amplitude of the high-frequency wave is much larger than that of the low-frequency one. We report here simulation results which suggest that there exists another important process for the transfer of energy from high- to low-frequency ion acoustic

waves. That is, an ion acoustic wave with lower frequency is generated from the wave packet of a high-frequency carrier wave. It grows up within several periods of oscillation of the amplitude of the original wave packet.

In our simulations, the wave was excited by an initial ion distribution function of the form

$$f(x, v) = (n_0/(2\pi)^{1/2} v_T)\{1+[1-\varepsilon_m \cos(k_m x)]\ \varepsilon \cos(k_0 x)\}$$
$$\times \exp\{-[v-(1-\varepsilon_m \cos(k_m x))\varepsilon v_p \cos(k_0 x)]^2/2v_T^2\} \quad . \quad (8)$$

Here ε, ε_m, k_0 and k_m are the amplitude of the excited ion acoustic wave, the amplitude of the modulation, the wave-number of the carrier wave, and the wavenumber of the modulation, respectively. Also, v_p is the approximate phase velocity of the ion acoustice wave, i.e., $v_p=\{(T_e/M)[3T_i/T_e+1/(1+k_0^2\lambda_{De}^2)\}^{1/2}$. It is observed that the distribution function of eq.(8) excites a backward wave as well as a forward one. The amplitude of the backward wave is, however, small in comparison with that of the forward wave, the ratio of their amplitudes being about 0.1. Therefore, the effects of the backward wave are considered negligible.

Figure (1) shows the time evolution of the wave packet thus excited. The parameters in eq.(8) are taken to be $\varepsilon_m=1.0$, $k_m/k_{De}=0.1$, $k_0/k_{De}=1.0$, and $T_e/T_i=20$. The amplitude, ε, is 0.08 in region $L/4\leq x\leq L/2$, and is zero in $0\leq x\leq L/4$ and $L/2\leq x\leq L$. Therefore, initially, the wave packet exists only in $L/4\leq x\leq L/2$. In Fig.(1a), the ion density profiles are depicted in the frame moving with velocity v_p. From $\omega_{pi}t=0$ to $\omega_{pi}t=60$, we can

clearly see the amplitude oscillation, which occurs only in the region of large amplitude. Then, the amplitude oscillation causes a deformation of the wave packet; for instance, at $\omega_{pi}t=20$ and 60, the top of the envelope is flattened due to the amplitude oscillation. The amplitude oscillation is not seen clearly after a few periods of the oscillation. At $\omega_{pi}t\simeq 50$, in the front part of the envelope there appears a long-wavelength perturbation. The propagation velocity of this perturbation is observed to be almost equalt to c_s, the ion acoustic velocity. As is well known, c_s is given approximately by $c_s=\{(T_e/M)(3T_i/T_e+1)\}^{1/2}$. Because the sound speed, c_s, is faster than both the group velocity and the phase velocity of the carrier wave with $k_0=k_{De}$, the long pulse gradually passes ahead of the wave packet. Figure (1b) gives the Fourier amplitudes of the ion density, $n_i(x)$, corresponding to Fig.(1a). The Fourier components with small wavenumbers are produced and grow in a rather short time scale ($\omega_{pi}t=30\simeq 40$). We note that the growth time of the long-wavelength waves is of the order of the period of the amplitudes oscillation. Figure (1c) shows the evolution of the density profile $n_L(x)$ from which the short-wavelength components are eliminated. That is, the density profile $n_L(x)$ is constructed only from Fourier components n_k of the real density $n_i(x)$ whose wavenumbers are smaller than one-half of the wavenumber of the carrier wave:

$$n_L(x) = \sum_{k\neq 0}^{k_0/2} \{n_k \exp(ikx) + c.c.\} \quad . \tag{9}$$

The long-wavelength perturbation $n_L(x)$ is not seen at $\omega_{pi}t=0$ in

Fig.(1c), but it has appeared at $\omega_{pi}t=10$. It is generated in the region where the original wave packet exists. Also, note that $n_L(x)$ is positive in the rising part of the envelope of the original wave packet and negative in the falling part. Its characteristic wavelength is about the size of the wave packet. It grows rapidly until $\omega_{pi}t=30\approx40$, after which the peak value of $n_L(x)$ does not vary significantly. Its propagation velocity is observed to be almost equal to the sound velocity c_s.

Figure (2a) plots the ion density $n_i(x)$ from $\omega_{pi}t=170$ to $\omega_{pi}t=200$. In this stage, the temporal variations in the amplitudes of the long-wavelength pulse and the wave packet are very slow. Since the velocity of the long-wavelength pulse is greater than that of the wave packet with $k_0\approx k_{De}$, the distance between the two gradually becomes larger. Just behind the long pulse, a transition region is formed in which the wavelength of the perturbation is shorter than that of the long-wavelength pulse but longer than that of the carrier wave of the original wave packet. This region links the long-wavelength pulse and the original wave packet with shorter wavelength. Figure (2b) shows the Fourier amplitudes, $|n_k|$, corresponding to Fig.(2a). We see that $|n_k|$ has three peaks. The peak at $k\approx k_0$ corresponds to the original wave packet, the peak with small k corresponds to the long-wavelength pulse, and the one in the intermediate region corresponds to the perturbations of the transition part in Fig.(2a).

Figure (3) illustrates the evolution of the ion distribution function, f(x, v, t). In the laboratory frame, when particles

with positive velocities are in a region of $\partial n_i/\partial x > 0$, which means that the electric field is positive, they are accelerated and gain kinetic energy, whereas those particles in regions where $\partial n_i/\partial x < 0$ lose kinetic energy. This acceleration and deceleration is clearly seen in Fig.(3) at $\omega_{pi}t=0$ and $\omega_{pi}t=14.4$. The vortices in phase space formed by the trapped particles after one period of amplitude oscillation are shown in Fig.(3) at $\omega_{pi}t=28,8$. At $\omega_{pi}t=57.6$, we see detrapped particles as well as trapped particles. Note that the former are produced mainly in the rising part of the envelope. The nonuniformity of the number of detrapped particles may play an important role in the generation of the long-wavelength waves.

In Fig.(4), peak values of the long-wavelength density pulse n_L are plotted as a function of time. Growing and saturation are clearly seen. The growth rate and the saturated peak value are large when the initial amplitude, ε, of the original wave packet is large. When we plot the peak values of n_L given in Fig.(4) as a function of $\omega_B t$, we obtain Fig.(5). Here ω_B is the bounce frequency of the ions and is given by

$$\omega_B = (k_0 eE_0/M)^{1/2} = \{k_0{}^2\lambda_{De}{}^2\varepsilon/(1+k_0{}^2\lambda_{De}{}^2)\}^{1/2}\omega_{pi} \quad ,(10)$$

where E_0 is the initial field strength. The peak values of n_L are normalized by the peak value of n_L at $(\omega_B/2\pi)t=0.36$. We note that in the early growing stage, i.e., $(\omega_B/2\pi)t \lesssim 1.5$, the growth of the normalized peak values is almost independent of the initial amplitude ε of the orginal wave packet. That is, the growth time of the long-wavelength waves is of the order of the period $2\pi/\omega_B$. This implies that the generation of the long

waves is mainly due to the resonance particles with $v \approx v_p$. In Fig.(6), the dependence of the saturated peak values on the initial amplitude ε is plotted. It is seen that the saturated peak values varies as ε^2. That is, the growth time is of the order of $2\pi/\omega_B$, whereas the saturated peak value is proportional to ε^2. Fig.(7) gives the temporal evolution of the long-wavelength perturbations, in which the temperature ratio T_e/T_i is chosen to be 30, 20, and 15 with the other parameters the same. More of the long-wavelength perturbations are generated when T_e/T_i is small.

So far we have investigated the properties of a wave packet which, at $\omega_{pi}t=0$, exists only in the region $L/4 \leq x \leq L/2$ and does not exist in other regions $0 \leq x \leq L/4$ and $L/2 \leq x \leq L$. Next, let us study the generation of long-wavelength waves from a periodically modulated wave. An example of such an initial ion density profile is illustrated in Fig.(8). The envelope of the original wave varies periodically with the rate of the modulation, ε_m. We examined the evolution of long-wavelength for several values of ε_m, with the other parameters being unchanged. The results are given in Fig.(9) which shows clearly that the long-wavelength wave is more generated when the rate of modulation, ε_m, is large. Hence, for this type of generation of long-wavelength waves, it is essential that the amplitude of the original wave be nonuniform in space. The modulation of the amplitude of the original wave leads to a spatial change in the number of trapped particles. The number of detrapped particles also has spatial variation. The nonumiformity of the number of these resonance particles may

have a significant influence on the formation of the long-wavelength waves.

§4. Discussions

Our computer simulations have shown that waves of long wavelength are generated from the wave packet of a short-wavelength ion acoustic wave and that these long-wavelength waves have a significant influence on the nonlinear evolution of the original wave packet. The characteristic wavelength of these waves is of the the order of the length of the wave packet. They grow during the first few periods of the amplitude oscillation in the region of large amplitude of the packet. Their growth rate is roughly proportional to the square root of the amplitude, $\varepsilon^{1/2}$, of the original wave, while the saturated peak value is proportional to ε^2. When the original wave is monochromatic and without modulation, generation of long-wavelength waves was not observed; therefore, spatial modulation of the amplitude of the original wave is essential for the generation of these waves.

Possible mechanisms for the generation of these long-wavelength waves from the original ion acoustic wave with shorter wavelength may be, for instance, the nonlinear Landau damping, the beam instability of the detrapped particles, particles reflected by the envelope, and resonance particles with $v \approx v_p$. The growth rates for the nonlinear Landau damping[2),11),12)] and for the beam instability[13)] are estimated to be too small, and hence they could not be the dominant

process for this type of wave generation. Tajiri[14] has calculated the density due to reflection of ions by the envelope of a modulated ion acoustic wave. The velocity range of such reflected particles is given by $|v-v_g| \sim 0(\varepsilon)$, where v_g is the group velocity. The low-frequency density perturbation due to the reflected particles is then of the order ε^2. The characteristic time for its formation is also of order ε^2, which is long in comparison with the time scale of the generation of the long-wavelength waves observed in our simulations. Consequently, neither is particle reflection by the envelope an important mechanism for this wave generation process.

The velocity range of the trapped particles in given by $|v-v_p| \sim 0(\varepsilon^{1/2})$. It is well known that these particles cause an amplitude oscillation when the wave amplitude is not so small. Some of the trapped particles are detrapped, because the wave does not completely recover its initial amplitude after one period of the amplitude oscillation. Furthermore, in the case of the modulated wave with its propagation in the positive x-direction, the detrapped paricles can be produced even if the wave amplitude does not change with time. In the rising portion of the envelope, part of the resonantly accelerated particles can be detrapped because the potential barrier is lower in front. Their velocity is, of course, faster than the phase velocity. On the other hand, in the falling portion of the envelope, only the decelerated particles can be detrapped due to the nonuniformity of the amplitude. When the distribution

function has a negative slope, $\partial f/\partial v<0$, for positive v, the number of the resonantly accelerated particles is larger than that of the decelerated ones. Accordingly, the detrapped particles are mainly produced in the rising part. These particles could be the origin of the long-wavelength ion acoustic waves. The damping and amplitude oscillation may increase the number of the detrapped particles. If the long-wavelength waves are due to these resonant particles, the characteristic time for thier formation would be of the order of a few bounce periods, and the density perturbation would be positive in the rising part of the wave packet. This corresponds with the results of our simulations, which would therefore imply that this type of generation of long-wavelength waves from a wave packet is mainly due to the resonance particles with $v \simeq v_p$. However, further theoretical and experimental studies[15)] would be needed for a complete understanding of these pheneomena.

Acknowledgements

The authors gratefully acknowledge Professors. T. Taniuti, Y. H. Ichikawa, K. Nishikawa and H. Ikezi for helpful discussions and suggestions. They are also grateful to Dr. J. Van Dam for his critical reading of this manuscript and to the members of the computer center of the Institute of Plasma Physics, Nagoya University, for their assistance with the computer simulations.

References

1) K. Shimizu and Y. H. Ichikawa: J. Phys. Soc. Japan 33 (1972) 789.

2) Y. H. Ichikawa and T. Taniuti: J. Phys. Soc. Japan 34 (1973) 513.

3) H. Ikezi, K. Schwarzenegger, A. L. Simons, Y. Ohsawa and T. Kamimura: submitted to the Phys. Fluids.

4) Y. Ohsawa and T. Kamimura: Research Report of Institute of Plasma Physics, Nagoya University, IPPJ-266 (1976).

5) J. Denavit: J. Computational Phys. 9 (1972) 75.

6) A. B. Langdon: J. Computational Phys. 6 (1970) 247.

7) J. M. Dawson: Phys. Rev. 118 (1960) 381.

8) P. H. Sakanaka,C. K. Chu and T. C. Marshall: Phys. Fluids 14 (1971) 611.

9) R. J. Mason: Phys. Fluids 14 (1971) 1934.

10) R. Z. Sagdeev and A. A. Galeev: Nonlinear Plasma Theory, edited by T. M. O'Neil and D. L. Book (Benjamin, New York, 1969), Chap. I.

11) K. Nishikawa: J. Phys. Soc. Japan 29 (1970) 449.

12) H. Ikezi and Y. Kiwamoto: Phys. Rev. Lett. 27 (1971) 718, see also Chap. III in reference 10.

13) see for instance, A. B. Mikhailovskii: Theory of Plasma Instabilities, translated by J. B. Barbour (Consultants Bureau, New York - London, 1974) Chap. I.

14) M. Tajiri: J. Phys. Soc. Japan 41 (1976) 1014.

15) Quite recently, N. Sato et al. experimentally observed the nonlinear wave packet which has very similar wave form to that observed by us. N. Sato, K. Saeki, and R. Hatakeyama: Phys. Rev. Lett. 38 (1977) 1480.

Figure Captions

Fig.1. Evolution of the ion acoustic wave with $T_e/T_i=20$, $k_0=k_{De}$, and $\varepsilon=0.08$. (a) Ion density profiles, n_i, in the wave frame; the abscissa is $x-v_p t$ with $v_p>0$. (b) Fourier amplitudes $|n_k|$ of n_i. (c) Density profiles n_L constructed from the long-wavelength Fourier components n_k with $k\leq k_0/2$ according to eq.(9). The vertical scale is magnified three times that of (a).

Fig.2. Evolution of the ion acoustic wave from $\omega_{pi}t=170$ to $\omega_{pi}t=200$. (a) Ion density profiles n_i. (b) Fourier amplitudes $|n_k|$ of n_i.

Fig.3. The ion distribution, f, in phase space. Contours of $\log(f/f_{max})$ are plotted, where f_{max} is the maximum value of the Maxwellian distribution. The top trace in each diagram indicates $f/f_{max}=0.002$, and contours equally divide $\log(f/f_{max})$ from $\log(0.002)$ to maximum of $\log(f/f_{max})$. The parameters are the same as those of Figs.(1) and (2).

Fig.4. Peak values of the long-wavelength density n_L versus time $\omega_{pi}t$. Peak values are normalized by the initial amplitude, ε, of the original wave packet.

Fig.5. Normalized peak values of n_L versus $\omega_B t$, where the bounce frequency ω_B is given by eq.(10). The peak values are normalized by the peak values at $(\omega_B/2)t=0.36$.

Fig.6. Saturated peak values of n_L as a function of the initial amplitude, ε, of the original wave packet. Dots and triangles are simulation results. k_m is the wavenumber

of the modulation and is defined in eq.(8). $T_e/T_i=20$; $k_0/k_{De}=1$.

Fig.7. Fourier amplitudes of the long-wavelength waves, $\sum_{k\neq 0}^{k_0/2}|n_k|$, versus time, $\omega_{pi}t$.

Fig.8. Example of a periodically modulated ion density at $\omega_{pi}t=0$.

Fig.9. Peak values of n_L normalized by ε versus $\omega_{pi}t$ for the modulated density of Fig.8. ε'_m is the rate of modulation, which appears in eq.(8). $T_e/T_i=20$; $k_0/k_{De}=1$; $\varepsilon=0.08$.

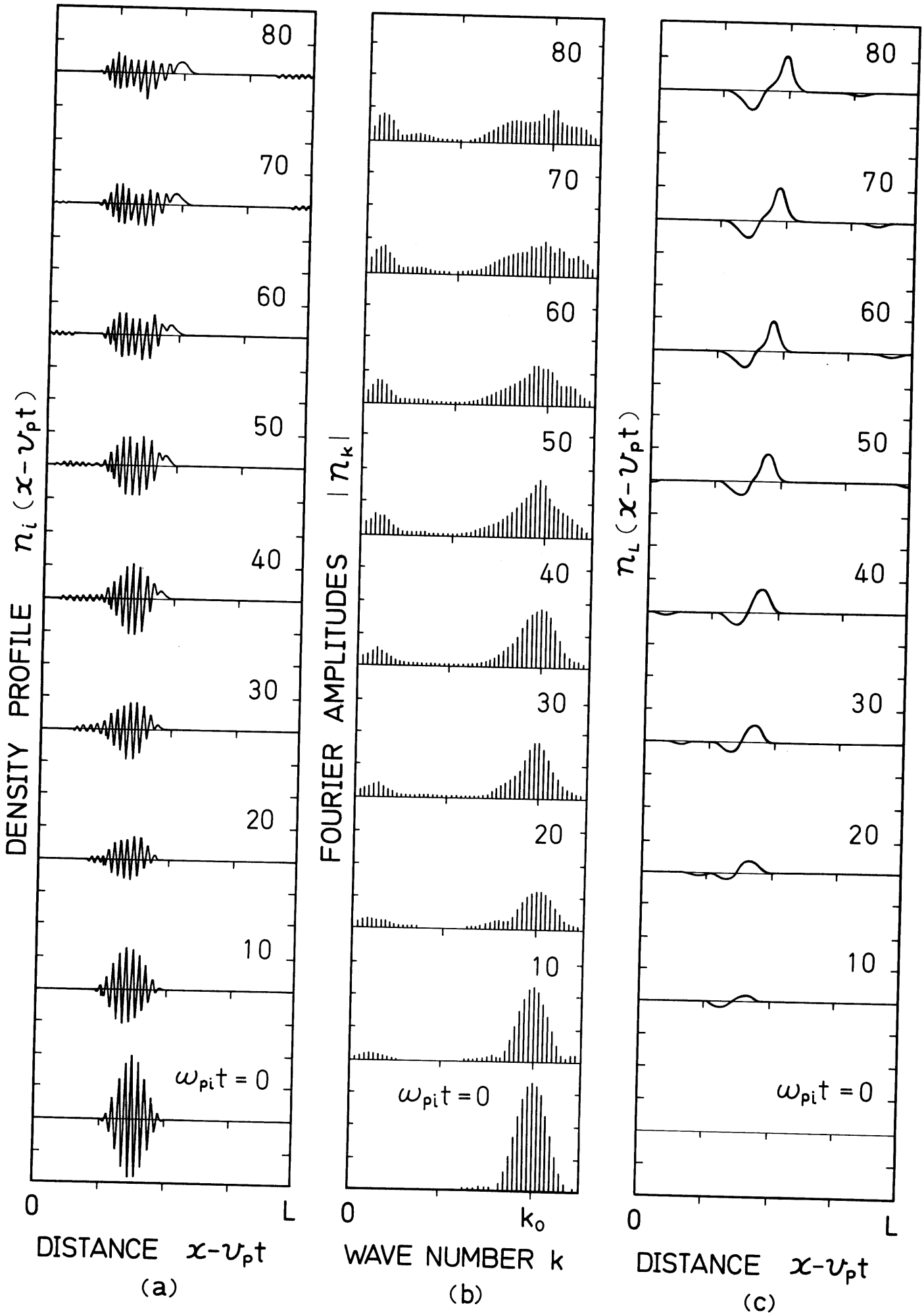
DENSITY PROFILE $n_i(x-v_pt)$
80
70
60
50
40
30
20
10
$\omega_{pi}t = 0$
0
L
DISTANCE $x-v_pt$
(a)
FOURIER AMPLITUDES $|n_k|$
80
70
60
50
40
30
20
10
$\omega_{pi}t = 0$
0
k_0
WAVE NUMBER k
(b)
$n_L(x-v_pt)$
80
70
60
50
40
30
20
10
$\omega_{pi}t = 0$
0
L
DISTANCE $x-v_pt$
(c)

Fig.1

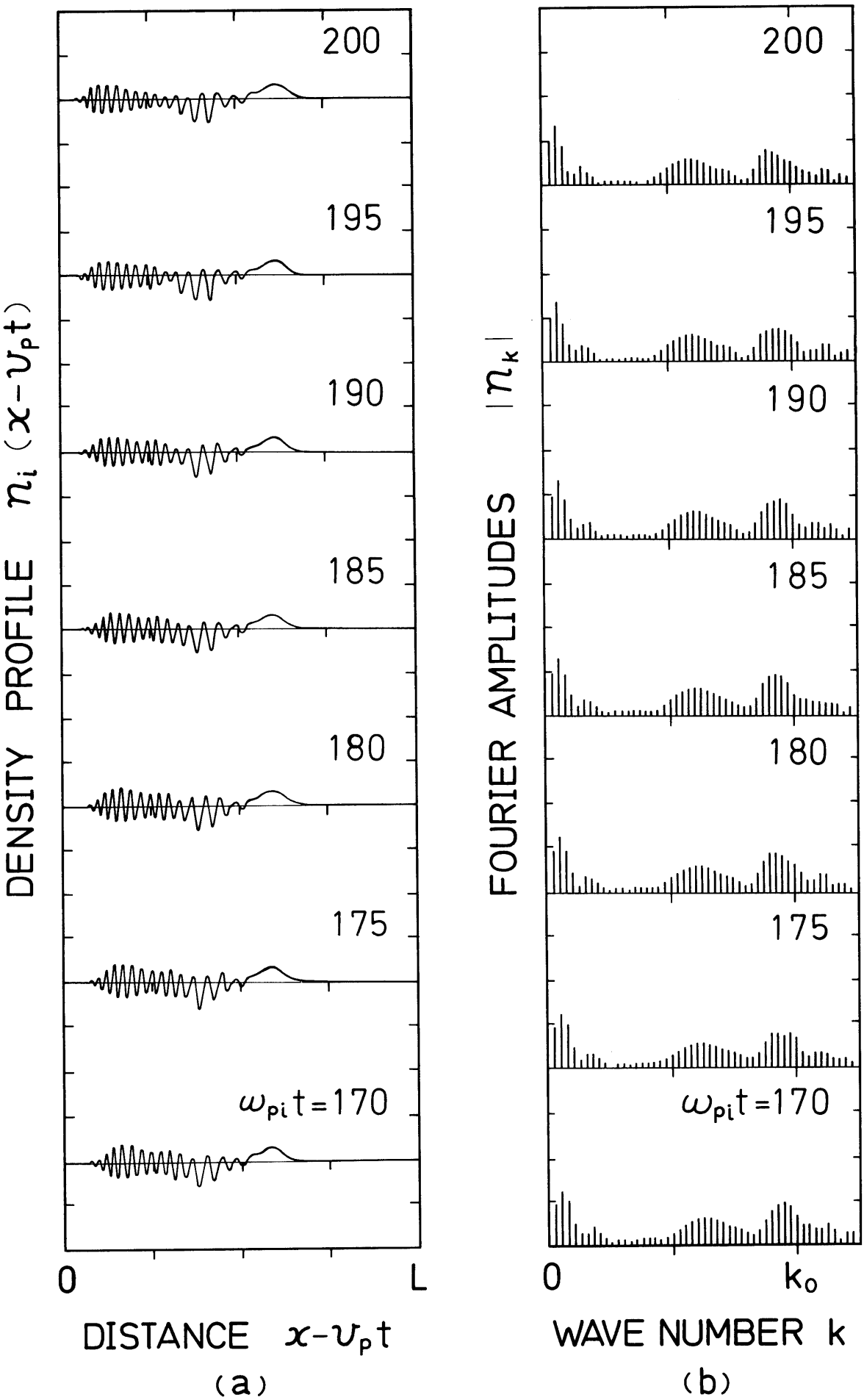
200
195
190
185
180
175
$\omega_{pi}t=170$
DENSITY PROFILE $n_i(x-v_pt)$
0
L
DISTANCE $x-v_pt$
(a)
FOURIER AMPLITUDES $|n_k|$
0
k_0
WAVE NUMBER k
(b)

Fig.2

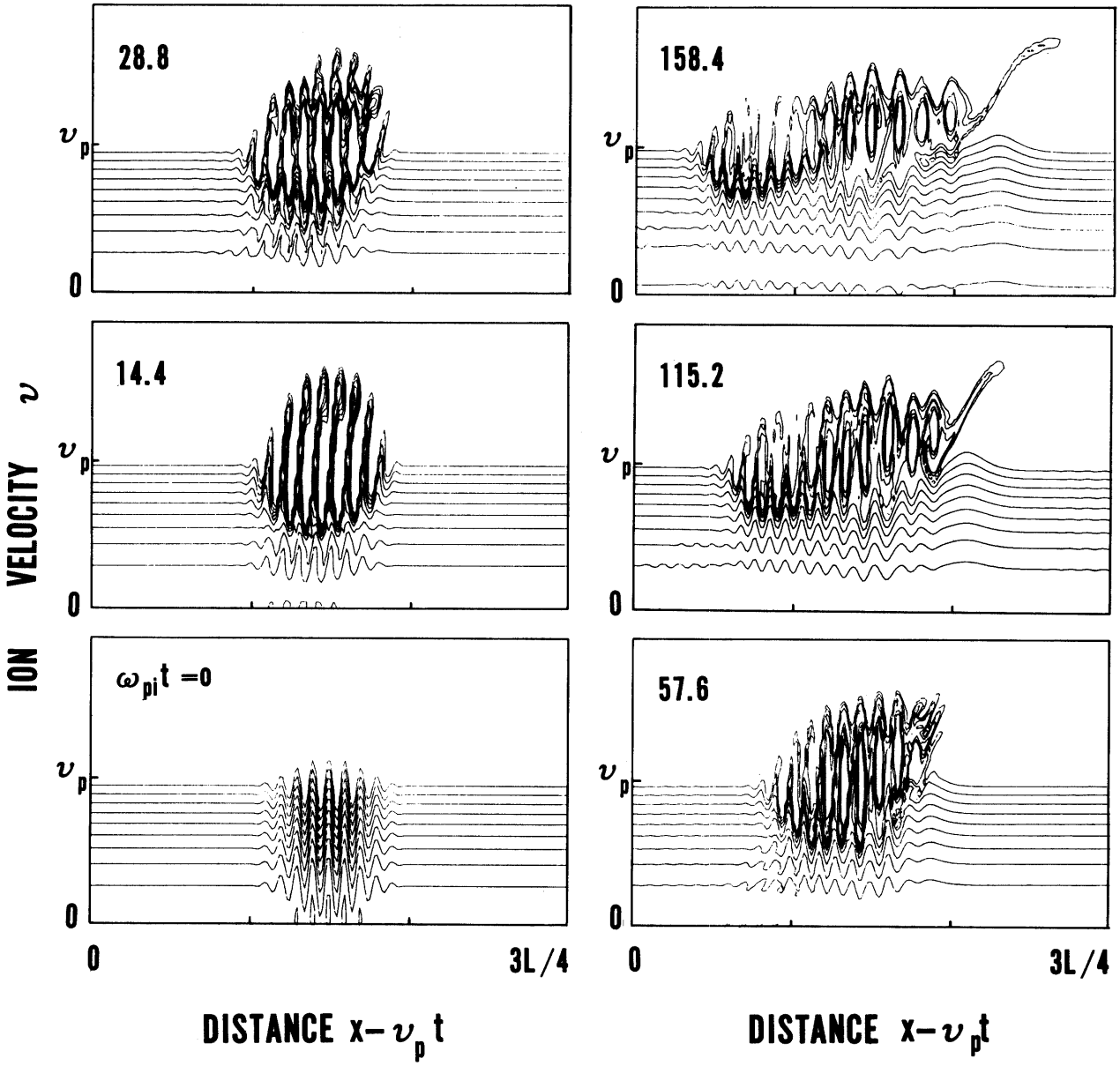
28.8
158.4
14.4
115.2
$\omega_{pi}t$ =0
57.6
v_p
0
ION VELOCITY v
0
3L/4
DISTANCE $x-v_p t$

Fig.3

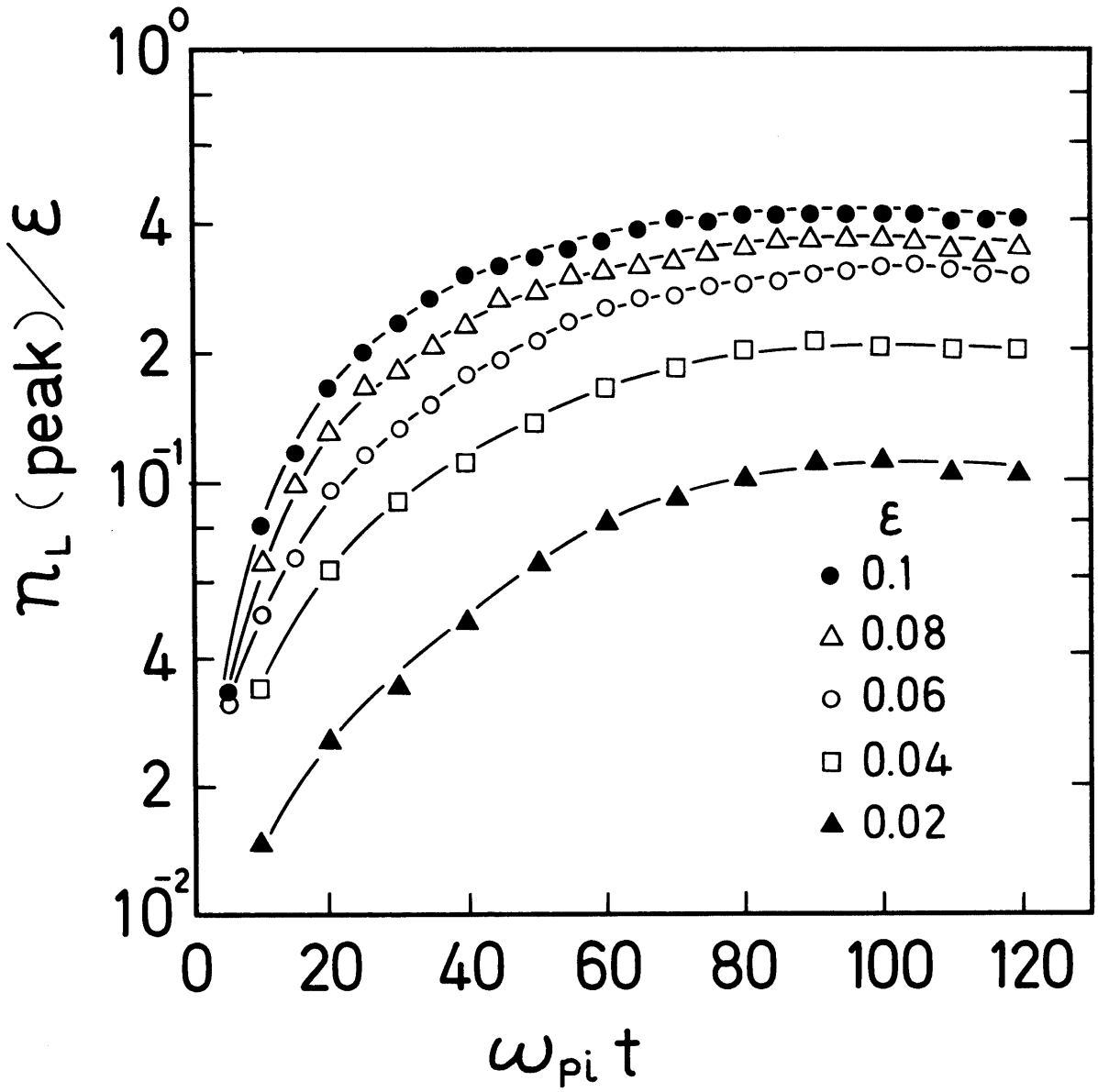
10^0
4
2
10^{-1}
4
2
10^{-2}
η_L (peak) / ε
0
20
40
60
80
100
120
ω_{pi} t
ε
0.1
0.08
0.06
0.04
0.02

Fig.4

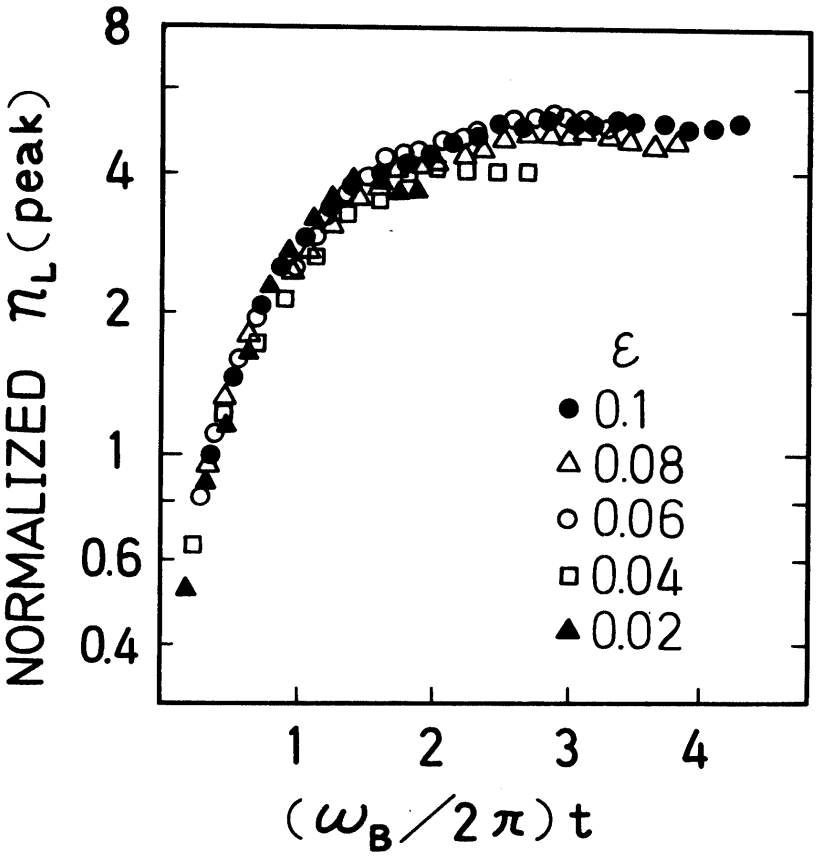
8
4
2
1
0.6
0.4
NORMALIZED η_L (peak)
1
2
3
4
$(\omega_B/2\pi)t$
ε
0.1
0.08
0.06
0.04
0.02

Fig.5

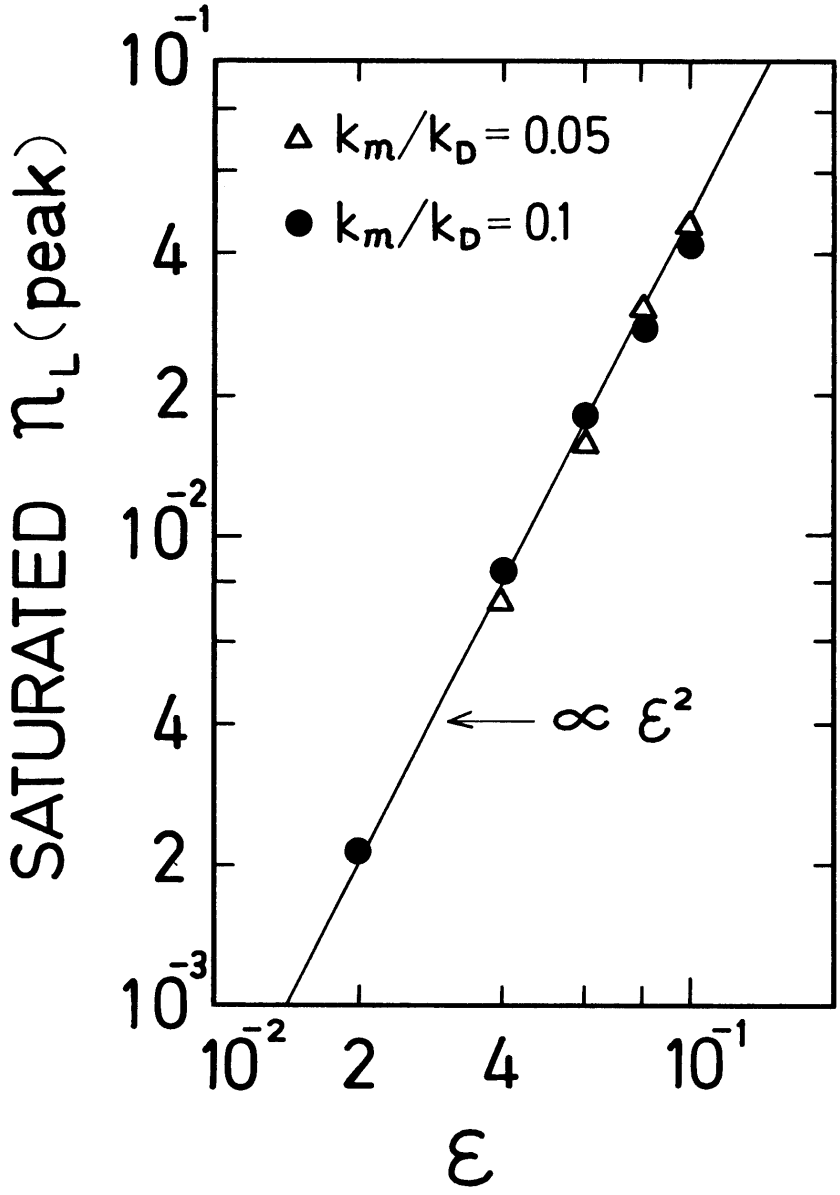
SATURATED η_L (peak)
10^{-1}
4
2
10^{-2}
4
2
10^{-3}
10^{-2}
2
4
10^{-1}
ε
△ $k_m/k_D = 0.05$
● $k_m/k_D = 0.1$
$\propto \varepsilon^2$

Fig.6

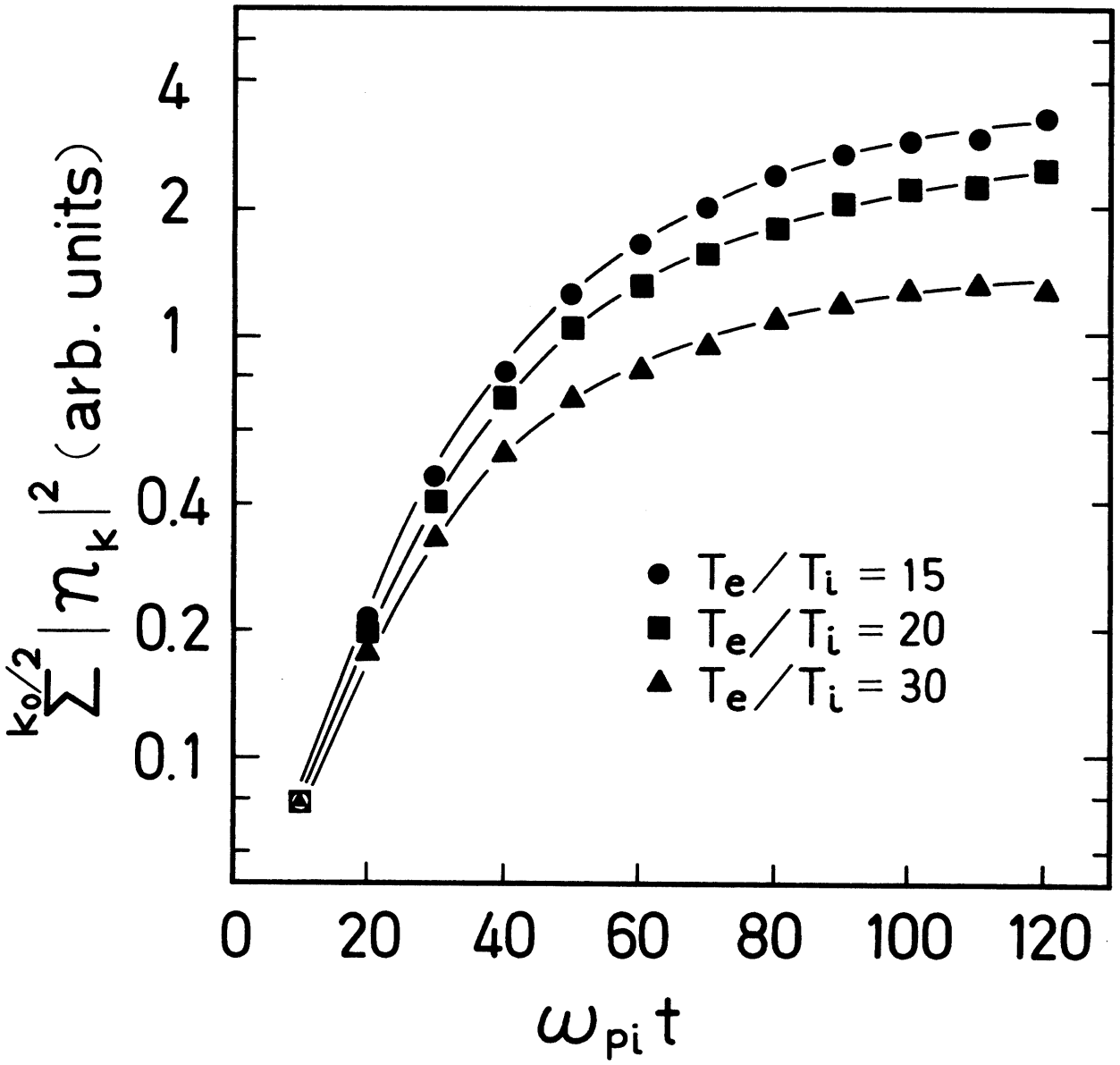
4
2
1
0.4
0.2
0.1
$\sum_{k_0/2} |n_k|^2$ (arb. units)
$T_e/T_i = 15$
$T_e/T_i = 20$
$T_e/T_i = 30$
0
20
40
60
80
100
120
$\omega_{pi} t$

Fig.7

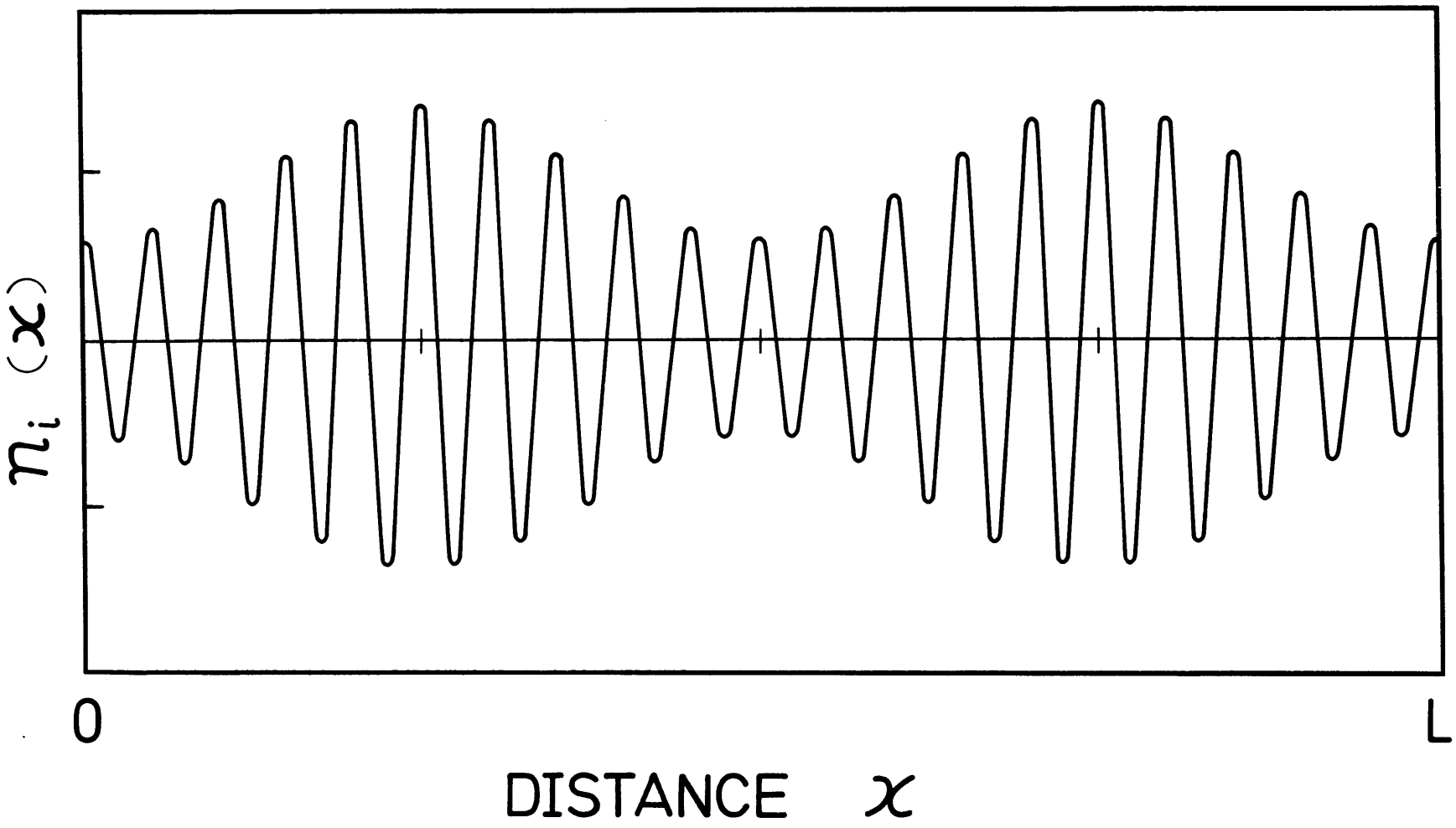

Fig.8

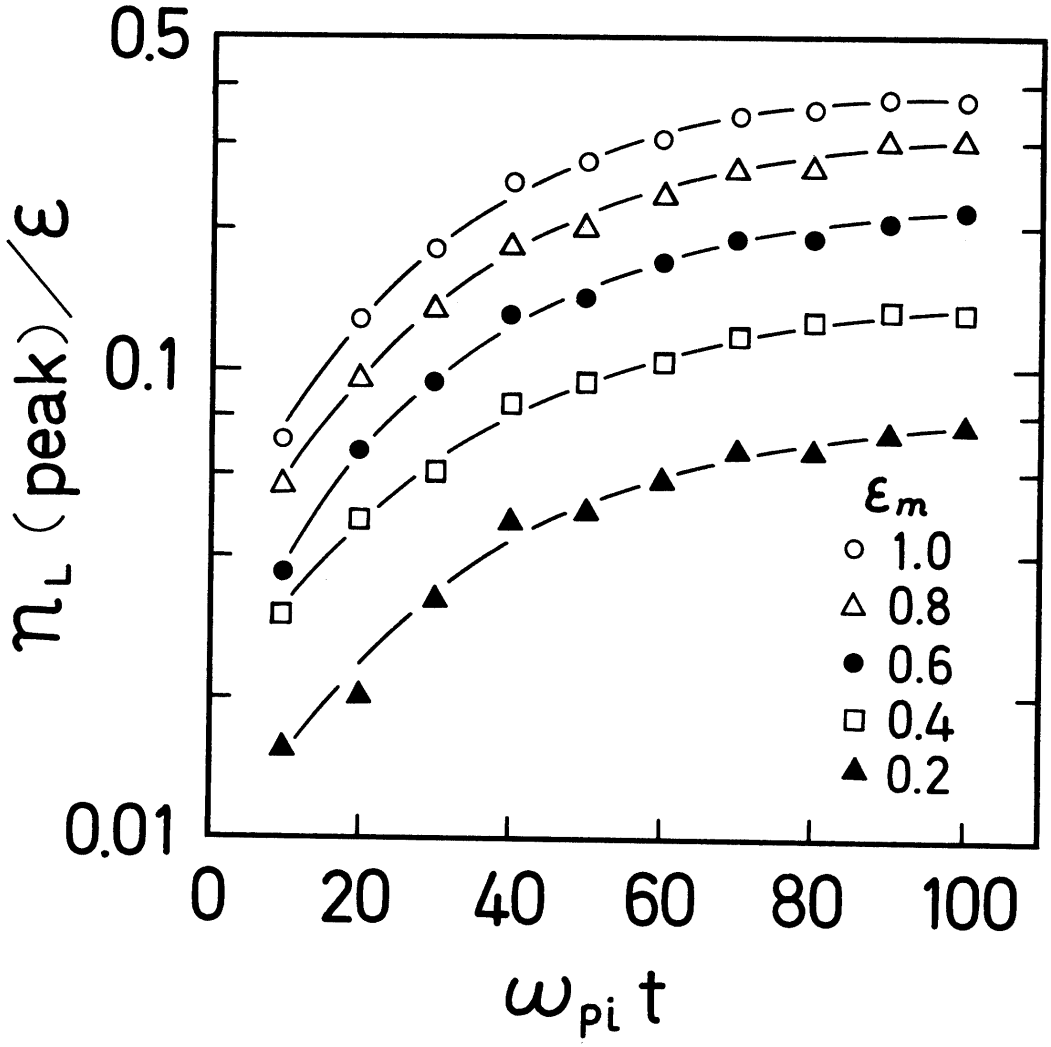
0.5
0.1
0.01
0
20
40
60
80
100
η_L (peak) / ε
ω_{pi} t
ε_m
1.0
0.8
0.6
0.4
0.2

Fig.9